Diamond micro-chip for quantum microscopy

Cite as: AVS Quantum Sci. **6**, 044405 (2024); doi: 10.1116/5.0223774
Submitted: 17 June 2024 · Accepted: 13 November 2024 ·
Published Online: 9 December 2024

Shahidul Asif,[1] Hang Chen,[2] Johannes Cremer,[3,4] Shantam Ravan,[3,4,5] Jeyson Támara-Isaza,[2,3,6] Saurabh Lamsal,[2] Reza Ebadi,[3,5] Yan Li,[1] Ling-Jie Zhou,[7] Cui-Zu Chang,[7] John Q. Xiao,[2] Amir Yacoby,[4,8] Ronald L. Walsworth,[3,5,9,a)] and Mark J. H. Ku[1,2,a)]

AFFILIATIONS

[1]Department of Materials Science and Engineering, University of Delaware, Newark, Delaware 19716, USA
[2]Department of Physics and Astronomy, University of Delaware, Newark, Delaware 19716, USA
[3]Quantum Technology Center, University of Maryland, College Park, Maryland 20742, USA
[4]Department of Physics, Harvard University, Cambridge, Massachusetts 02138, USA
[5]Department of Physics, University of Maryland, College Park, Maryland 20742, USA
[6]Departamento de Física, Universidad Nacional de Colombia, 110911 Bogotá, Colombia
[7]Department of Physics, Pennsylvania State University, University Park, Pennsylvania 16802, USA
[8]John A. Paulson School of Applied Sciences and Engineering, Harvard University, Cambridge, Massachusetts 02138, USA
[9]Department of Electrical and Computer Engineering, University of Maryland, College Park, Maryland 20742, USA

[a)]**Authors to whom correspondence should be addressed:** walsworth@umd.edu and mku@udel.edu

ABSTRACT

The nitrogen-vacancy (NV) center in diamond is an increasingly popular quantum sensor for microscopy of electrical current, magnetization, and spins. However, efficient NV–sample integration with a robust, high-quality interface remains an outstanding challenge to realize scalable, high-throughput microscopy. In this work, we characterize a diamond micro-chip (DMC) containing a (111)-oriented NV ensemble and demonstrate its utility for high-resolution quantum microscopy. We perform strain imaging of the DMC and find minimal detrimental strain variation across a field of view of tens of micrometer. We find good ensemble NV spin coherence and optical properties in the DMC, suitable for sensitive magnetometry. We then use the DMC to demonstrate wide-field microscopy of electrical current and show that diffraction-limited quantum microscopy can be achieved. We also demonstrate the deterministic transfer of DMCs with multiple materials of interest for next-generation electronics and spintronics. Lastly, we develop a polymer-based technique for DMC placement. This work establishes the DMC's potential to expand the application of NV quantum microscopy in materials, device, geological, biomedical, and chemical sciences.

INTRODUCTION

Nitrogen-vacancy (NV) centers in diamond are a leading modality for sensitive, high-spatial-resolution measurements of magnetic fields. NV-diamond sensors operate under ambient and also extreme conditions (of temperature, pressure, etc.) and have wide-ranging applications in the physical and life sciences, from condensed matter physics and material science[1,2] to chemistry,[3] biomedical science,[4] geology,[5] and circuit analysis.[6–8]

One common approach to NV magnetic field imaging is scanning probe microscopy (SPM), typically employing a probe consisting of a single NV near the tip of a diamond nanostructure.[9] SPM spatial resolution is limited only by the stand-off distance d between the NV and the sample; this enables resolution as small as tens of nanometer.[10] However, SPM necessarily involves slow pixel-by-pixel scanning, may scratch the sample,[11] and is not suitable for liquid or soft matter samples. Furthermore, SPM involves significant cost and complexity, including common NV probe degradation (e.g., picking up dirt or the single NV trapped in the wrong charge state) and the need for high degree of vibration isolation and temperature stability. Another implementation of NV magnetic field imaging is NV wide-field microscopy, using a modality known as the quantum diamond microscope (QDM).[12,13] Here, a surface layer of an NV ensemble on a macroscopic diamond crystal is utilized. With a suitable application of microwave (MW) fields to manipulate the NV spins, a measurement of the spatial distribution of the magnetic field across the NV ensemble layer is encoded in the emitted pattern of NV photoluminescence (PL), which

is imaged with a camera. The QDM features parallel acquisition of magnetic field information across an entire field of view (i.e., no scanning), which enables high-throughput microscopy of both solid and liquid/soft samples.[14,15] Spatial resolution as small as $\sigma \sim 150\,\text{nm}$,[15] limited by optical diffraction, can be achieved. While this resolution is coarser than from NV-SPM, nevertheless sub-micrometer resolution suffices for a large number of applications. Additionally, there is room for further improvement, e.g., via inhomogeneous ensemble control[15] and machine learning.[16] Given the aforementioned features, the QDM provides a powerful means for high-throughput, high-resolution microscopy for diverse applications.[5–8,14,17–21]

In order to achieve diffraction-limited QDM magnetic imaging resolution σ of a sample of interest, it is necessary to ensure a small NV layer stand-off distance from the sample $d \ll \sigma$. NVs at a depth $\sim$10 nm can be created reliably without significant detriment to their properties,[22] and hence, d is primarily determined by how well the diamond contacts the sample. However, creating high-quality diamond–sample interface remains an outstanding challenge that hinders the wider application of the QDM. Depositing the sample material or fabricating the target device directly on the bulk diamond crystal can ensure close proximity between the NVs and the sample, but this approach is possible only for a limited number of materials, e.g., for van der Waals materials that can be placed on diamond via exfoliation or polymer-based transfer[17,19,23–27] or for materials that can be grown on diamond, e.g., via evaporation[28] or sputtering. When working with materials for which this option is not available, a diamond–sample interface has typically been realized by simply placing the bulk diamond crystal ($\sim$mm in dimensions) in direct contact with the sample. However, with such a large contact area, there is necessarily non-uniform flatness and particles (e.g., dust) invariably get trapped in between the diamond and the sample, leading to a large and inhomogeneous d across the NV layer that limits the resolution to no better than a few micrometer.[5,13,29] Furthermore, imaging through diamond, which has a high index of refraction, leads to aberration that can further degrade resolution.[5]

A promising approach to these issues is to fabricate a small and thin diamond structure to ensure good diamond–sample interface.[30–32] Here, we report the development and characterization of an optimized diamond micro-chip (DMC) for use in ensemble NV magnetic imaging. Each DMC is tens of micrometer in lateral dimension and 1–2 μm in thickness and provides a high-quality interface for the NV sensing layer with both solid-state samples and liquid-phase materials via microfluidics[33,34] [Fig. 1(a)]. In past work, DMCs with lateral dimension ranging from hundreds to tens of micrometer and thickness less than few micrometer were used for quantum optics[35–40] and NV sensing applications.[7,32,41–43] However, several key features of DMCs, necessary for many QDM applications, remain to be demonstrated, including: ensemble NV spin coherence and optical properties similar to that in high-quality bulk diamond; sufficiently uniform strain across the NV layer, to not limit NV sensor performance;[17,44–48] diffraction-limited sub-micrometer magnetic imaging resolution; a (111)-oriented NV ensemble, to enable use of a vertical bias magnetic field; and reliable, deterministic placement of the DMC on the sample of interest. In this work, we realize DMCs with all these desired properties; outline their deposition and manipulation; characterize their properties; and, as an example DMC application, perform sensitive wide-field magnetic imaging of electrical current. We also discuss possible future uses of DMCs.

RESULT

DMC fabrication and positioning begins with a protocol reported in Refs. 37–39. An array of DMCs are created with lateral dimensions 10×10, 20×20, and $50 \times 50\ \mu\text{m}^2$, and thickness $\sim$1–2 μm. Each chip is attached to a diamond mainframe via a small bridge. Nitrogen implantation at an energy of 10 keV with appropriate dosage creates an ensemble NV surface layer with a density [NV] $\sim 1000\,\mu\text{m}^{-2}$ and average depth $\sim$10 nm. DMCs are fabricated from single-crystal CVD diamond substrate with (111) orientation, which leads to one class of NVs with quantization axis, set by the substitutional nitrogen and the vacancy, along the vertical (z) direction.

To detach a single DMC and subsequently position it at a target location, we employ a sharp tip on a micro-positioner [Figs. 1(b) and 1(d)]. The diamond mainframe containing the DMC array, with the NV surface facing down, is attached to a 3D translational stage and a tilt stage, which enables one to bring the DMC array close to the substrate; this ensures the NV surface remains face down when the desired single DMC is detached. When this DMC is broken off, part of the bridge remains on the chip. The off-center position of the bridge introduces chirality, and once a DMC has landed at the target location, one can confirm that the NV surface is down by looking at the location of the bridge and comparing it to the image of the chip prior to detachment [Fig. 1(e)]. We used this procedure to show that single DMCs with ensemble (111) NV layers can be integrated with a diverse range of materials of interest for next-generation electronics and spintronics [Figs. 1(e) and 1(i)]: yttrium iron garnet grown via liquid-phase epitaxy, a magnetic insulator with low magnon damping; magnetically doped topological insulator hosting quantum anomalous Hall effects[49,50] grown via molecular beam epitaxy; altermagnet RuO_2 (Refs. 51–53) Hall-bar device; a thin flake (<10 nm thick) of 50% Co-substituted Fe_5GeTe_2, which is a room-temperature van der Waals antiferromagnet;[54] and a superconducting Josephson junction, often used as a qubit building block.

In ensemble NV magnetometry—using optically detect magnetic resonance (ODMR) and related NV measurement techniques—one typically applies an external bias magnetic field B_0 along a particular NV axis so to be optimally sensitive to the component of the sample magnetic field B_z parallel to this axis. (A discussion of the NV spin Hamiltonian, ensemble NV measurement techniques, and the effects of strain and off-axis magnetic fields is given in Ref. 55.) However, ensemble NV magnetometry to date has predominantly been performed with diamonds having (100) crystal orientation, including work using DMCs.[7,32,41–43] (100) diamond has all four NV axes oriented at 54.7° with respect to the vertical, which is typically inconvenient and/or non-optimal for many applications, particularly in materials science.[56] In this work, we solve this problem by using DMCs fabricated from (111) orientation diamond, with one NV axis along the vertical direction.

NV-diamond–sample fabrication can lead to modification of the local strain environment[17,44,46] with inhomogeneous strain being detrimental to NV magnetometry.[45,47,57] Thus, we characterize the spatial profile of the effective strain field $M_z(x, y)$ in example DMCs by QDM strain microscopy of the (111)-oriented NVs, using the technique described in Refs. 44, 45, and 47 (further details described in supplementary material). In Fig. 2, we show the measured M_z profile of two characteristic $10 \times 10\ \mu\text{m}^2$ DMCs. Two observations can be made immediately. First, the variation of M_z is generally below 1 MHz within

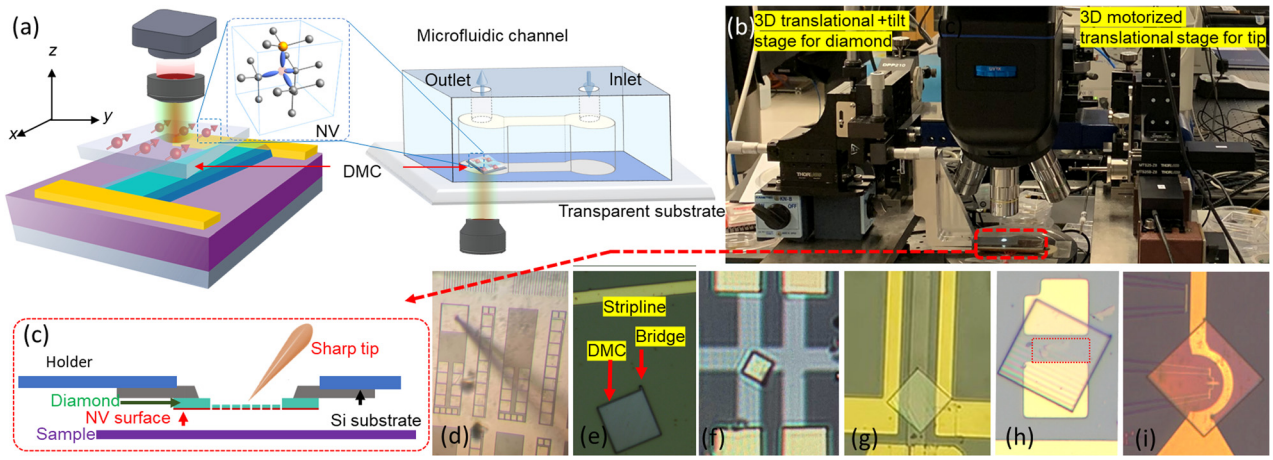

FIG. 1. (a) A diamond micro-chip (DMC), with tens of micrometer lateral dimension and 1–2 μm thickness, enables a high-quality ensemble NV–sample interface. A DMC contains an ensemble of NVs in a surface layer (tens of nanometer thick), which enables wide-field magnetic imaging with a camera—a modality known as the quantum diamond microscope (QDM). Each DMC employed in this work contains (111)-oriented NVs (inset), which allows the application of an out-of-plane bias magnetic field B_0 and measurement of an out-of-plane component of the sample magnetic field B_z. A DMC can also be conveniently integrated with a microfluidic device. (b)–(d) Schematics for depositing a single DMC in target location. Diamond–sample containing arrays of DMCs is mounted to a Si substrate attached to a holder. The holder is manipulated with a 3D translational and tilt stage, which serves to bring the desired DMC array into the field of view of a microscope and above the location where a single DMC is to be deposited. A sharp tip controlled by a 3D motorized translational stage is used to detach the desired DMC and subsequently nudges it to the target location. (b) Deposition apparatus with a microscope, stages for the diamond and tip, and holder (diamond and sample is underneath the holder). (c) Cartoon schematic of the deposition process. (d) Microscope image of a tip near a DMC. An array of DMCs with sizes 50 × 50, 20 × 20, and 10 × 10 μm^2 is visible; each DMC is attached to a diamond mainframe via a narrow bridge. A sharp tip detaches the desired single DMC and then subsequently nudges this DMC into the target location. (e) The bridge that previously connected a DMC with the diamond mainframe introduces chirality and enables one to confirm that the NV side is indeed facing downward. (e)–(i) DMC can be deposited on a diverse range of materials of interest for next-generation electronics and spintronics: (e) yttrium iron garnet (YIG) thin-film next to an MW stripline; (f) magnetically doped topological insulator Hall-bar device; (g) altermagnet RuO_2 Hall-bar device; (h) <10-nm-thick flake (flake highlighted by the dashed rectangle) of 50% Co-substituted Fe_5GeTe_2, a room-temperature van der Waals antiferromagnet; and (i) a Josephson junction.

the bulk of the DMC. Furthermore, a dramatic strain profile associated with lattice dislocations, such as observed in Ref. 45, is absent. To provide a more quantitative assessment of the strain characteristics, we examine the statistics of the measured M_z. A histogram of M_z [Figs. 2(c) and 2(d)] shows a mono-modal distribution. Ensemble NV sensing requires that the spread of the measured M_z is small in each DMC; i.e., there is an overall, homogeneous strain environment in each chip. The standard deviation is $\Delta M_z = 0.1$ and 0.033 MHz for the two DMCs, corresponding to a fractional strain of 3×10^{-6} and 1×10^{-6}, respectively, and comparable to the state-of-the-art value of 1×10^{-6} found in the quiet area of a bulk single-crystal diamond.[58] This result demonstrates that fabricated DMC has favorable strain profile not too different from that of a bulk single-crystal diamond. Furthermore, these results show that it is possible to fabricate a thin diamond structure and be able to maintain sufficiently low strain variation on the order of $\sim 10^{-6}$, which is a necessary ingredient for a proposed approach[58] to use strain microscopy in diamond for directional detection of WIMPS, a candidate form of dark matter. (Detailed discussion in supplementary material.)

Next, we characterize the spin coherence properties of the (111)-oriented NVs in an example DMC. Figure 3(a) shows a measured NV ODMR spectrum, with a resolved hyperfine splitting due to ^{14}N nuclear spins; and a linewidth (half-width half-maximum) of about 1.2 MHz that is comparable to NVs in bulk diamond generated at a similar density and implantation energy.[22] For the same DMC, we also measure an ensemble NV Hahn-echo spin coherence time $T_2 \approx 2.3$ μs [Fig. 3(b)] and a longitudinal spin relaxation time $T_1 \approx 0.46$ ms [Fig. 3(c)]. For shallow NVs (~tens of nanometer), T_2 and T_1 decrease rapidly with NV depth d. For a standard (100)-oriented diamond, simulations using stopping range of ions in matter (SRIM)[59] estimate an average stopping range of the nitrogen ion to be ~15 nm for an implantation energy of 10 keV.[60,61] However, for (111)-oriented diamond, SRIM finds that the stopping range can be reduced by as much as a factor of 2;[62] hence, $d \sim 10$ nm or below may be expected for NVs in the present DMC. To estimate d, we refer to the measurement performed in Ref. 63, which reports T_1 and T_2 of several shallow NVs with experimentally characterized d. Using these results, a typical NV depth $d \sim 8$ nm best corresponds to the measured combination of NV $T_1 \sim 0.5$ ms and $T_2 \sim 2$ μs in our DMC. This value is consistent with the measurement reported in Ref. 22, where $T_2 \sim 2.5$ μs is found for an NV ensemble with $d \sim 10$ nm. Hence, we conclude that the ensemble NV spin coherence properties in the present DMC are consistent with those at a similar depth and density in standard bulk diamond crystal.

As an application demonstration, we perform high-resolution wide-field NV magnetic imaging using a 20 × 20 μm^2 DMC deposited on a fabricated meandering wire phantom, through which we send a DC current to generate a target magnetic field [Fig. 4(a)]. The (111)-oriented DMC allows us to directly measure B_z, the z-component of the phantom magnetic field. Figure 4(b) shows a simulated B_z map, based on a model of current flow through the phantom. The measured B_z map is shown in Fig. 4(c), in reasonable agreement with the simulation, other than for a small area around the corners where complexity in the real current flow is likely present and not captured by the model.

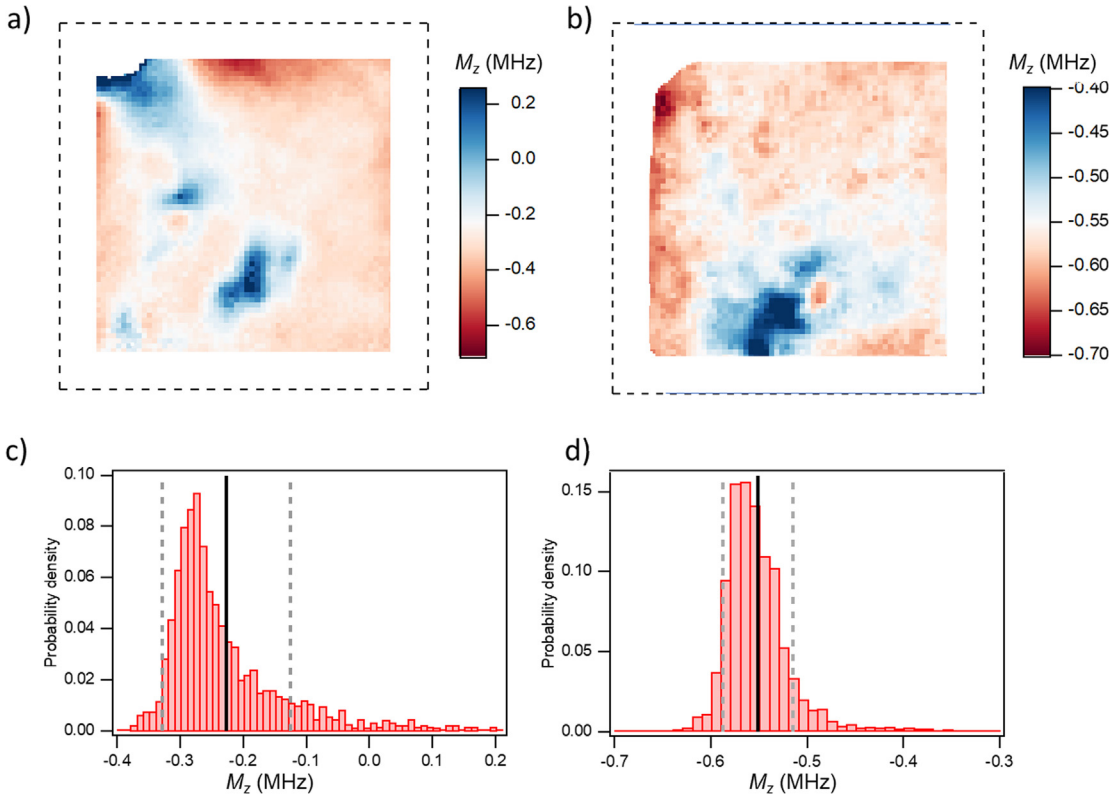

Fig. 2. Measured distribution of axial strain field M_z reveals variation of local strain experienced by (111)-oriented NVs in DMC. (a) and (b) M_z maps from two different DMCs with lateral dimensions of $10 \times 10\ \mu m^2$. Dashed edges show DMC boundaries. Strain image pixel size is $0.14\ \mu m$. (c) and (d) Histograms of M_z values from DMCs shown in (a) and (b), respectively. Mean $\overline{M_z}$ and standard deviation ΔM_z are $\overline{M_z} = -0.2$ MHz, $\Delta M_z = 0.1$ MHz for the DMC shown in (a), and $\overline{M_z} = -0.55$ MHz, $\Delta M_z = 0.033$ MHz for the DMC shown in (b). Mean and one standard deviation values are shown in the histograms as solid and dashed lines, respectively.

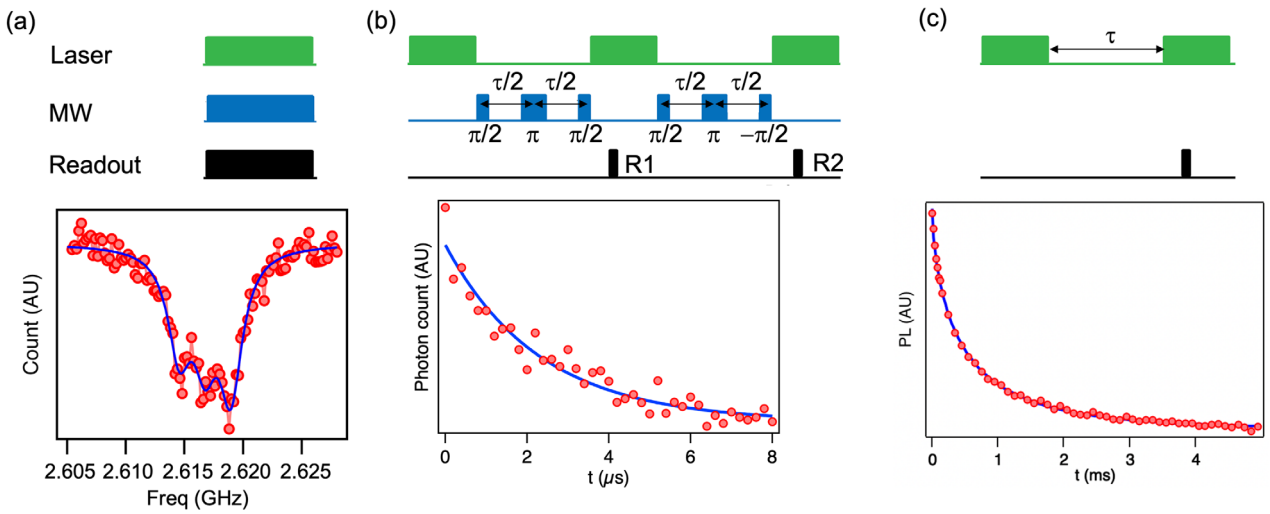

Fig. 3. Spin coherence properties of (111)-oriented NVs in DMCs. The schematics of measurement sequence is shown in the top of each panel. (a) Optically detected magnetic resonance showing that hyperfine splitting is resolved, and linewidth (half-width half-maximum) is 1.18(6) MHz. (b) Hahn spin-echo measures $T_2 \approx 2.3(3)\ \mu s$. (c) Relaxometry measurement obtains a longitudinal relaxation time $T_1 \approx 0.46(4)$ ms.

To characterize the spatial resolution σ of ensemble NV fluorescence imaging using a DMC, we extract the minimum observable size of small features in the DMC strain map of M_z. Figure 4(d) shows an example, with two strain features in close proximity. We fit M_z to two Gaussian profiles and determine the size of the smaller feature to be 450(30) nm, consistent with the expected diffraction-limited spatial resolution of about 440 nm (supplementary material).

A key to DMC utility is to be able to conveniently and reliably place the chip at the desired location relative to the target sample. When a DMC detaches, it is not possible to control precisely where it lands; hence, most often it will be some distance away from the target. The common approach is then to push or drag the DMC to the desired location using a sharp tip.[7,32,37–39,42,43] However, this technique has a high probability of damaging the sample or rendering the tip and/or DMC unusable (e.g., by picking up dirt or the DMC becoming stuck). Thus, the present fully-tip-based method is non-optimal for high-throughput DMC applications.

Inspired by van der Waals (vdW) material assembly, we employ a polymer-assisted dry-transfer process for DMC manipulation, summarized in Figs. 5(a)–5(e) (details discussed in supplementary material). With a sharp tip, we first break a DMC off from the diamond mainframe onto a substrate (this may be a separate substrate from the target sample). We then use a patterned polymer microstructure on a transparent thin glass slide to pick up the DMC and bring it to the desired location on the target sample. To release the DMC, we tilt the slide so that the chip is gradually detached from the polymer microstructure. Finally, a tip can be used for fine-tuning of DMC placement; as there is no need for the DMC to traverse a long distance, little movement is required for the tip, and hence, there is minimal risk to the sample, tip, and DMC. In Figs. 5(f)–5(l), we show the sequence applied to the deposition of a 50×50 μm^2 DMC on a RuO_2 altermagnet device. We note that recently, Ref. 42 also demonstrated a different dry-transfer technique to place a similarly sized DMC on vdW materials. Compared to that work, our technique has the following features (see supplementary material for further details): (i) there is no need to heat the sample, which is desirable for temperature- or air-sensitive materials; (ii) no additional fabrication procedure is needed; and (iii) instead of being permanently attached to the target sample, the DMC

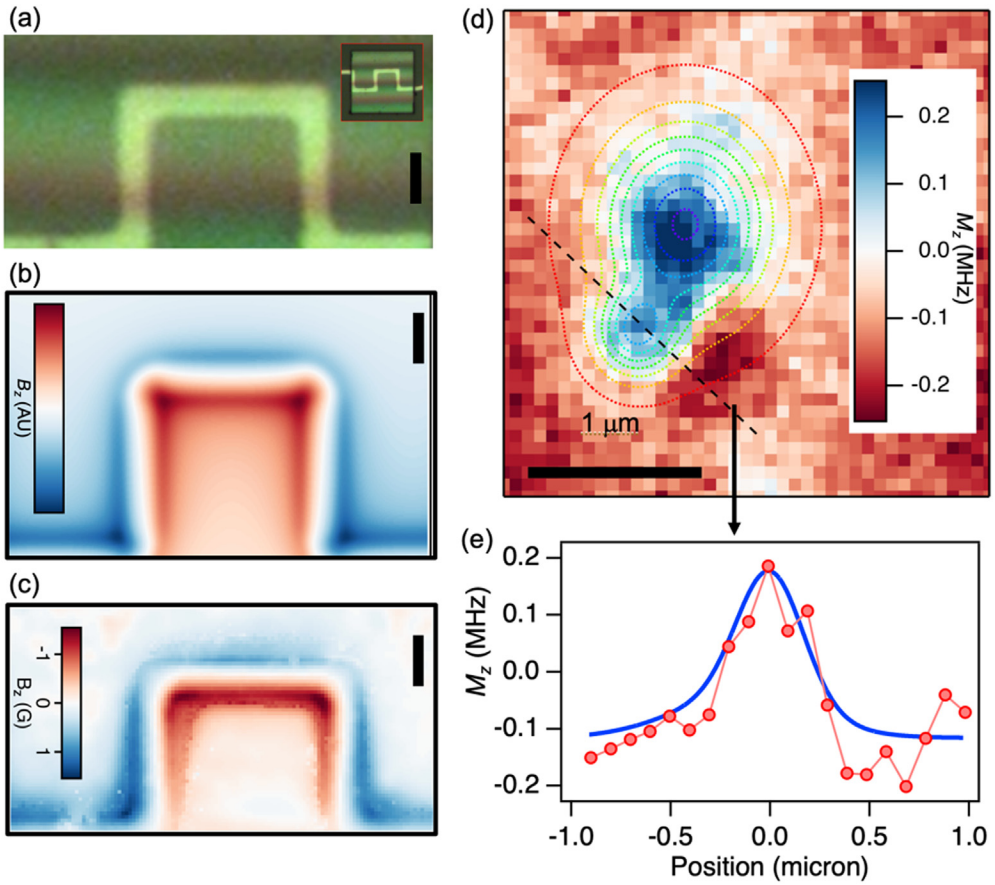

FIG. 4. Demonstration of wide-field magnetic imaging using (111)-oriented NVs in a 20×20 μm^2 DMC. (a) Optical image of a meandering phantom as seen through a DMC. Inset: DMC is deposited on a fabricated meandering wire phantom. (b) Simulated vertical (z) component of magnetic field B_z generated by DC current in phantom. (c) Ensemble NV map of B_z measured with current in phantom. The overall pattern matches that of simulation in panel (b), with minor differences due to complexity in current flow around wire corners. Scale bar corresponds to 5 μm for (a)–(c). (d) Two localized features in axial strain field M_z used to benchmark spatial resolution of ensemble NV magnetic imaging using a DMC. M_z is fit to two Gaussians; contour of the two-dimensional fit is shown. (e) Linecut of M_z data (fit) along dashed line in (d) shown as red points (blue curve). Extracted spatial resolution is 450(30) nm.

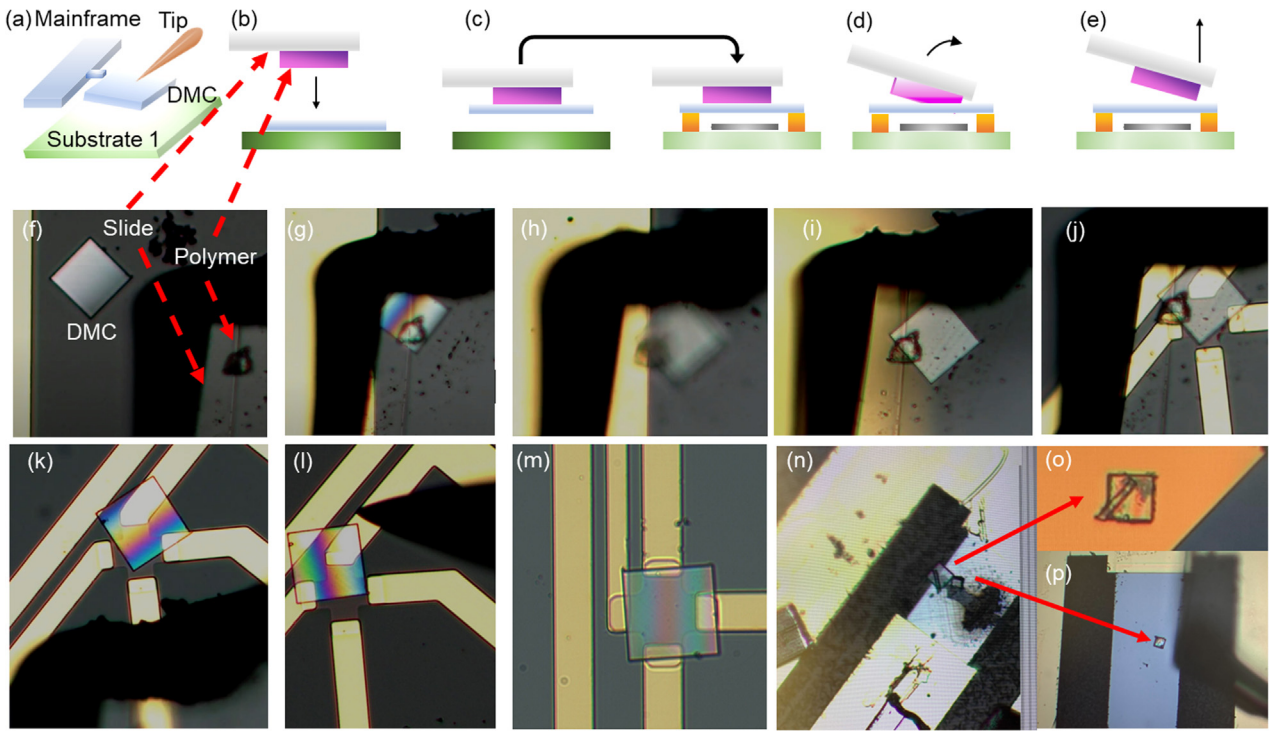

Fig. 5. Polymer-assisted dry-transfer technique for efficient DMC manipulation and placement. (a)–(e) Schematics. (a) A DMC is first broken off from the diamond mainframe (e.g., with a tip) and lands on a substrate. (b) A transparent substrate (e.g., a glass slide) with a polymer microstructure approaches the DMC. (c) The polymer assembly picks up the DMC and places it on a sample of interest. (d) Tilting the slide releases the DMC from the polymer. A docking structure with adhesive property can also further facilitate the release. (e) The polymer assembly is pulled off, leaving the DMC on the sample. (f)–(l) Optical images of the polymer DMC deposition process. (f) A DMC, after being broken off, sits on a substrate. In the image, one also sees a glass slide with a polymer microstructure. (g) The polymer assembly approaches and comes in contact with the DMC. (h-i) The polymer assembly picks up the DMC. (h) shows the optical image when the substrate is still in focus; the DMC is out of focus, showing that it is picked up. (i) shows the DMC in focus, whereas the substrate is no longer in focus. (j) The polymer assembly brings the DMC on top of a RuO_2 altermagnet Hall-bar device and deposits the DMC on the sample. (k) The polymer assembly exits, while the DMC remains on the sample. (l) A tip can be used to further fine-tune the DMC position. (m) The DMC from (l) is picked up again by polymer assembly and transferred to another RuO_2 Hall-bar device. (n)–(p) The technique can also selectively transfer an individual DMC from a collection of closely spaced chips. Among the two DMCs on a permalloy spin-torque device (n), one is transferred to an Au structure (o) and another transferred to a new spin-torque device (p).

can be reused. For example, the DMC in Fig. 5(l) was subsequently picked up again and transferred to another RuO_2 device [Fig. 5(m)]. Moreover, in Figs. 5(n)–5(p), we show that two DMCs, already placed on a permalloy spin-torque device, can be picked up again using a polymer microstructure and positioned on new devices; this result shows that we can selectively pick up an individual DMC from a collection of nearly spaced chips. We also have demonstrated the potential of this technique on different materials showing the successful deposition of diamond microchips on several materials (more details in supplementary material Secs. 6 and 7). This technique enables a reliable, high-throughput process where one first breaks off all the DMCs onto a substrate for storage, and then, one simply transfers an individual DMC from the storage substrate to the target sample, repeating the process for other DMCs and possibly other samples, as desired.

CONCLUSION

In conclusion, we characterize a diamond micro-chip (DMC) with a (111)-oriented NV ensemble in a nanoscale surface layer, and demonstrate its utility for high-resolution quantum microscopy. We find that the DMC has a suitably homogeneous strain profile and ensemble NV spin coherence properties consistent with NVs in bulk diamond at a similar depth from the surface. We perform high-resolution wide-field NV magnetic imaging using a DMC deposited on a wire phantom carrying a DC current and show that diffraction-limited resolution can be achieved for ensemble NV fluorescence imaging using a DMC. We also demonstrate the ability to interface a DMC with a diverse set of materials and discuss implications for diverse applications. Finally, we develop a polymer-based pick-and-place technique for reliable DMC manipulation and localization. Our work reveals the potential of DMCs with an (111)-oriented NV ensemble to expand the application of NV quantum sensing in wide-ranging fields such as materials, device, geological, biomedical, and chemical sciences.

SUPPLEMENTARY MATERIAL

See the supplementary material for provided separately in the supplementary materials section. It has seven subsections and provides additional insight and information without disrupting the flow of the main manuscript by being added in a supplementary section. The first subsection describes the robustness of the diamond micro-chip in its

applications. The second subsection briefly describes the experimental setup used in this work. The third subsection includes a short discussion on microscopy of strain and stray field. Subsection four is dedicated to explaining the proposal of the dark matter detection application using the strain tracks in diamond. In subsection five, we discussed the spatial resolution relevant to the application of our technique. In the last two subsections, we gave a detailed explanation of how the "polymer-assisted dry transfer" method works and the prospect of the technique in different materials and surfaces.

ACKNOWLEDGEMENTS

This work was supported by NSF Award No. 2203829, the University of Delaware Research Foundation—Strategic Initiative award, J.C., S.R., R.E., and R.L.W. Acknowledge support from the Army Research Laboratory MAQP program under Contract No. W911NF-19-2-0181, and from the Quantum Technology Center and Joint Quantum Institute at the University of Maryland. This research was partially supported by NSF through the University of Delaware Materials Research Science and Engineering Center No. DMR-2011824 Seed Award program. J.T.-I. acknowledges support from the Universidad Nacional de Colombia, Project No. 57522. The quantum anomalous Hall insulator growth and fabrication done at Penn State is supported by the ARO Award (No. W911NF2210159). C.-Z.C. acknowledges the support from Gordon and Betty Moore Foundation's EPiQS Initiative (No. GBMF9063 to C.-Z.C.). A.Y. acknowledges support from the Army Research Office under Grant No. W911NF-22-1-0248, the Gordon and Betty Moore Foundation through Grant No. GBMF 9468, and by the Quantum Science Center (QSC), a National Quantum Information Science Research Center of the U.S. Department of Energy (DOE). The authors thank Xi Wang (University of Delaware) and Philip Kim (Harvard University) for providing probe stations for diamond micro-chip deposition. The authors thank Andrew F. May and Michael A. McGuire for providing the Co-substituted Fe_5GeTe_2 crystals, Nikola Maksimovic for fabricating the Josephson junction, Xinhao Wang for growing RuO_2, and Tristan Timog and Matthew Coughlin for experimental support.

AUTHOR DECLARATIONS

Conflict of Interest

The authors have no conflicts to disclose.

Author Contributions

Shahidul Asif and Hang Chen contributed equally to this work.

Shahidul Asif: Conceptualization (equal); Data curation (equal); Formal analysis (equal); Investigation (equal); Methodology (equal); Visualization (equal); Writing – original draft (equal); Writing – review & editing (equal). **Hang Chen:** Conceptualization (equal); Data curation (equal); Formal analysis (equal); Investigation (equal); Methodology (equal); Visualization (equal); Writing – original draft (equal); Writing – review & editing (equal). **Johannes Cremer:** Data curation (supporting); Investigation (supporting); Writing – review & editing (supporting). **Shantam Ravan:** Data curation (supporting); Investigation (supporting). **Jeyson Tamara-Isaza:** Data curation (supporting). **Saurabh Lamsal:** Data curation (supporting). **Reza Ebadi:** Data curation (supporting); Investigation (supporting). **Yan Li:** Data curation (supporting). **Ling-Jie Zhou:** Data curation (supporting); Investigation (supporting). **Cui-Zu Chang:** Data curation (supporting); Investigation (supporting). **John Q. Xiao:** Funding acquisition (supporting); Resources (supporting). **Amir Yacoby:** Conceptualization (supporting); Project administration (supporting); Resources (supporting); Supervision (supporting); Visualization (supporting). **Ronald L. Walsworth:** Conceptualization (supporting); Funding acquisition (supporting); Methodology (supporting); Resources (supporting); Supervision (supporting); Visualization (supporting); Writing – review & editing (equal). **Mark J. H. Ku:** Conceptualization (equal); Formal analysis (equal); Funding acquisition (lead); Project administration (lead); Resources (lead); Visualization (equal); Writing – original draft (equal); Writing – review & editing (equal).

DATA AVAILABILITY

The data that support the findings of this study are available from the corresponding authors upon reasonable request.

REFERENCES

[1]F. Casola, T. van der Sar, and A. Yacoby, Nat. Rev. Mater. **3**, 17088 (2018).
[2]E. Marchiori, L. Ceccarelli, N. Rossi, L. Lorenzelli, C. L. Degen, and M. Poggio, Nat. Rev. Phys. **4**, 49 (2021).
[3]D. R. Glenn, D. B. Bucher, J. Lee, M. D. Lukin, H. Park, and R. L. Walsworth, Nature **555**, 351 (2018).
[4]N. Aslam, H. Zhou, E. K. Urbach, M. J. Turner, R. L. Walsworth, M. D. Lukin, and H. Park, Nat. Rev. Phys. **5**, 157 (2023).
[5]D. R. Glenn, R. R. Fu, P. Kehayias, D. Le Sage, E. A. Lima, B. P. Weiss, and R. L. Walsworth, Geochem. Geophys. Geosyst. **18**, 3254 (2017).
[6]M. Ashok, M. J. Turner, R. L. Walsworth, E. V. Levine, and A. P. Chandrakasan, ACM J. Emerg. Technol. Comput. Syst. **18**, 67 (2022).
[7]M. Garsi, R. Stöhr, A. Denisenko, F. Shagieva, N. Trautmann, U. Vogl, B. Sene, F. Kaiser, A. Zappe *et al.*, "Non-invasive imaging of three-dimensional integrated circuit activity using quantum defects in diamond," arXiv:2112.12242 (2021).
[8]M. J. Turner, N. Langellier, R. Bainbridge, D. Walters, S. Meesala, T. M. Babinec, P. Kehayias, A. Yacoby, E. Hu *et al.*, Phys. Rev. Appl. **14**, 014097 (2020).
[9]P. Maletinsky, S. Hong, M. S. Grinolds, B. Hausmann, M. D. Lukin, R. L. Walsworth, M. Loncar, and A. Yacoby, Nat. Nanotechnol. **7**, 320 (2012).
[10]K. Chang, A. Eichler, J. Rhensius, L. Lorenzelli, and C. L. Degen, Nano Lett. **17**, 2367 (2017).
[11]U. Vool, A. Hamo, G. Varnavides, Y. Wang, T. X. Zhou, N. Kumar, Y. Dovzhenko, Z. Qiu, C. A. C. Garcia *et al.*, Nat. Phys. **17**, 1216 (2021).
[12]E. V. Levine, M. J. Turner, P. Kehayias, C. A. Hart, N. Langellier, R. Trubko, D. R. Glenn, R. R. Fu, and R. L. Walsworth, Nanophotonics **8**, 1945 (2019).
[13]S. C. Scholten, A. J. Healey, I. O. Robertson, G. J. Abrahams, D. A. Broadway, and J.-P. Tetienne, J. Appl. Phys **130**, 150902 (2021).
[14]D. Le Sage, K. Arai, D. R. Glenn, S. J. DeVience, L. M. Pham, L. Rahn-Lee, M. D. Lukin, A. Yacoby, A. Komeili *et al.*, Nature **496**, 486 (2013).
[15]F. Ziem, M. Garsi, H. Fedder, and J. Wrachtrup, Sci. Rep. **9**, 12166 (2019).
[16]C. Qiao, D. Li, Y. Guo, C. Liu, T. Jiang, Q. Dai, and D. Li, Nat. Methods **18**, 194 (2021).
[17]D. A. Broadway, S. C. Scholten, C. Tan, N. Dontschuk, S. E. Lillie, B. C. Johnson, G. Zheng, Z. Wang, A. R. Oganov *et al.*, Adv. Mater. **32**, 2003314 (2020).
[18]H. C. Davis, P. Ramesh, A. Bhatnagar, A. Lee-Gosselin, J. F. Barry, D. R. Glenn, R. L. Walsworth, and M. G. Shapiro, Nat. Commun. **9**, 131 (2018).
[19]M. J. H. Ku, T. X. Zhou, Q. Li, Y. J. Shin, J. K. Shi, C. Burch, L. E. Anderson, A. T. Pierce, Y. Xie *et al.*, Nature **583**, 537 (2020).
[20]J. M. McCoey, M. Matsuoka, R. W. de Gille, L. T. Hall, J. A. Shaw, J.-P. Tetienne, D. Kisailus, L. C. L. Hollenberg, and D. A. Simpson, Small Methods **4**, 1900754 (2020).

[21]D. A. Simpson, R. G. Ryan, L. T. Hall, E. Panchenko, S. C. Drew, S. Petrou, P. S. Donnelly, P. Mulvaney, and L. C. L. Hollenberg, Nat. Commun. **8**, 458 (2017).
[22]J.-P. Tetienne, R. W. de Gille, D. A. Broadway, T. Teraji, S. E. Lillie, J. M. McCoey, N. Dontschuk, L. T. Hall, A. Stacey *et al.,* Phys. Rev. B **97**, 085402 (2018).
[23]H. Chen, S. Asif, M. Whalen, J. Támara-Isaza, B. Luetke, Y. Wang, X. Wang, M. Ayako, S. Lamsal *et al.,* 2D Mater. **9**, 025017 (2022).
[24]H. Chen, S. Asif, K. Dolui, Y. Wang, J. Támara-Isaza, V. M. L. D. P. Goli, M. Whalen, X. Wang, Z. Chen *et al.,* ACS Appl. Mater. Interfaces **15**, 3287 (2023).
[25]A. J. Healey, S. Rahman, S. C. Scholten, I. O. Robertson, G. J. Abrahams, N. Dontschuk, B. Liu, L. C. L. Hollenberg, Y. Lu *et al.,* ACS Nano **16**, 12580 (2022).
[26]N. J. McLaughlin, H. Wang, M. Huang, E. Lee-Wong, L. Hu, H. Lu, G. Q. Yan, G. Gu, C. Wu *et al.,* Nano Lett. **21**, 7277 (2021).
[27]N. J. McLaughlin, C. Hu, M. Huang, S. Zhang, H. Lu, G. Q. Yan, H. Wang, Y. Tserkovnyak, N. Ni *et al.,* Nano Lett. **22**, 5810 (2022).
[28]S. E. Lillie, D. A. Broadway, N. Dontschuk, S. C. Scholten, B. C. Johnson, S. Wolf, S. Rachel, L. C. L. Hollenberg, and J.-P. Tetienne, Nano Lett. **20**, 1855 (2020).
[29]I. Bertelli, J. J. Carmiggelt, T. Yu, B. G. Simon, C. C. Pothoven, G. E. W. Bauer, Y. M. Blanter, J. Aarts, and T. van der Sar, Sci. Adv. **6**, eabd3556 (2020).
[30]C. Du, T. van der Sar, T. X. Zhou, P. Upadhyaya, F. Casola, H. Zhang, M. C. Onbasli, C. A. Ross, R. L. Walsworth *et al.,* Science **357**, 195 (2017).
[31]H. Zhang, M. J. H. Ku, F. Casola, C. H. R. Du, T. van der Sar, M. C. Onbasli, C. A. Ross, Y. Tserkovnyak, A. Yacoby *et al.,* Phys. Rev. B **102**, 024404 (2020).
[32]Y. Schlussel, T. Lenz, D. Rohner, Y. Bar-Haim, L. Bougas, D. Groswasser, M. Kieschnick, E. Rozenberg, L. Thiel *et al.,* Phys. Rev. Appl. **10**, 034032 (2018).
[33]R. D. Allert, F. Bruckmaier, N. R. Neuling, F. A. Freire-Moschovitis, K. S. Liu, C. Schrepel, P. Schätzle, P. Knittel, M. Hermans *et al.,* Lab Chip **22**, 4831 (2022).
[34]M. Krečmarová, M. Gulka, T. Vandenryt, J. Hrubý, L. Fekete, P. Hubík, A. Taylor, V. Mortet, R. Thoelen *et al.,* ACS Appl. Mater. Interfaces **13**, 18500 (2021).
[35]X. Guo, N. Delegan, J. C. Karsch, Z. Li, T. Liu, R. Shreiner, A. Butcher, D. D. Awschalom, F. J. Heremans *et al.,* Nano Lett. **21**, 10392 (2021).
[36]X. Guo, M. Xie, A. Addhya, A. Linder, U. Zvi, T. D. Deshmukh, Y. Liu, IN. Hammock, Z. Li *et al.,* "Direct-bonded diamond membranes for heterogeneous quantum and electronic technologies," arXiv:2306.04408 (2023).
[37]D. Riedel, D. Rohner, M. Ganzhorn, T. Kaldewey, P. Appel, E. Neu, R. J. Warburton, and P. Maletinsky, Phys. Rev. Appl. **2**, 064011 (2014).
[38]D. Riedel, I. Söllner, B. J. Shields, S. Starosielec, P. Appel, E. Neu, P. Maletinsky, and R. J. Warburton, Phys. Rev. X **7**, 031040 (2017).
[39]D. Riedel, S. Flågan, P. Maletinsky, and R. J. Warburton, Phys. Rev. Appl. **13**, 014036 (2020).
[40]M. Ruf, M. IJspeert, S. van Dam, N. de Jong, H. van den Berg, G. Evers, and R. Hanson, Nano Lett. **19**, 3987 (2019).
[41]T. S. Ghiasi, M. Borst, S. Kurdi, B. G. Simon, I. Bertelli, C. Boix-Constant, S. Mañas-Valero, H. S. J. van der Zant, and T. van der Sar, "Nitrogen-vacancy magnetometry of CrSBr by diamond membrane transfer," arXiv:2307.01129 (2023).
[42]G. Q. Yan, S. Li, H. Lu, M. Huang, Y. Xiao, L. Wernert, J. A. Brock, E. E. Fullerton, H. Chen *et al.,* Adv. Mater. **34**, 2200327 (2022).
[43]J. Zhou, G. Q. Yan, M. Huang, N. J. McLaughlin, C. R. Du, and H. Wang, Appl. Phys. Lett. **123**, 024003 (2023).
[44]D. A. Broadway, B. C. Johnson, M. S. J. Barson, S. E. Lillie, N. Dontschuk, D. J. McCloskey, A. Tsai, T. Teraji, D. A. Simpson *et al.,* Nano Lett. **19**, 4543 (2019).
[45]P. Kehayias, M. J. Turner, R. Trubko, J. M. Schloss, C. A. Hart, M. Wesson, D. R. Glenn, and R. L. Walsworth, Phys. Rev. B **100**, 174103 (2019).
[46]S. Knauer, J. P. Hadden, and J. G. Rarity, npj Quantum Inf. **6**, 50 (2020).
[47]M. C. Marshall, R. Ebadi, C. Hart, M. J. Turner, M. J. H. Ku, D. F. Phillips, and R. L. Walsworth, Phys. Rev. Appl. **17**, 024041 (2022).
[48]M. C. Marshall, D. F. Phillips, M. J. Turner, M. J. H. Ku, T. Zhou, N. Delegan, F. J. Heremans, M. V. Holt, and R. L. Walsworth, Phys. Rev. Appl. **16**, 054032 (2021).
[49]W. Yuan, L.-J. Zhou, K. Yang, Y.-F. Zhao, R. Zhang, Z. Yan, D. Zhuo, R. Mei, M. H. W. Chan *et al.,* "Electrical switching of the edge current chirality in quantum anomalous hall insulators," arXiv:2205.01581 (2024).
[50]L.-J. Zhou, R. Mei, Y.-F. Zhao, R. Zhang, D. Zhuo, Z.-J. Yan, W. Yuan, M. Kayyalha, M. H. W. Chan *et al.,* Phys. Rev. Lett. **130**, 086201 (2023).
[51]A. Bose, N. J. Schreiber, R. Jain, D.-F. Shao, H. P. Nair, J. Sun, X. S. Zhang, D. A. Muller, E. Y. Tsymbal *et al.,* Nat. Electron. **5**, 267 (2022).
[52]L. Šmejkal, J. Sinova, and T. Jungwirth, Phys. Rev. X **12**, 031042 (2022).
[53]L. Šmejkal, J. Sinova, and T. Jungwirth, Phys. Rev. X **12**, 040501 (2022).
[54]A. F. May, M.-H. Du, V. R. Cooper, and M. A. McGuire, Phys. Rev. Mater. **4**, 074008 (2020).
[55]J. F. Barry, J. M. Schloss, E. Bauch, M. J. Turner, C. A. Hart, L. M. Pham, and R. L. Walsworth, Rev. Mod. Phys. **92**, 015004 (2020).
[56]D. Rohner, J. Happacher, P. Reiser, M. A. Tschudin, A. Tallaire, J. Achard, B. J. Shields, and P. Maletinsky, Appl. Phys. Lett. **115**, 192401 (2019).
[57]E. Bauch, C. A. Hart, J. M. Schloss, M. J. Turner, J. F. Barry, P. Kehayias, S. Singh, and R. L. Walsworth, Phys. Rev. X **8**, 031025 (2018).
[58]M. C. Marshall, M. J. Turner, M. J. H. Ku, D. F. Phillips, and R. L. Walsworth, Quantum Sci. Technol. **6**, 024011 (2021).
[59]J. F. Ziegler, Nucl. Instrum. Methods Phys. Res., Sect. B **219-220**, 1027 (2004).
[60]R. Fukuda, P. Balasubramanian, I. Higashimata, G. Koike, T. Okada, R. Kagami, T. Teraji, S. Onoda, M. Haruyama *et al.,* New J. Phys. **20**, 083029 (2018).
[61]D. M. Toyli, C. D. Weis, G. D. Fuchs, T. Schenkel, and D. D. Awschalom, Nano Lett. **10**, 3168 (2010).
[62]O. Lehtinen, B. Naydenov, P. Börner, K. Melentjevic, C. Müller, L. P. McGuinness, S. Pezzagna, J. Meijer, U. Kaiser *et al.,* Phys. Rev. B **93**, 035202 (2016).
[63]S. Sangtawesin, B. L. Dwyer, S. Srinivasan, J. J. Allred, L. V. H. Rodgers, K. De Greve, A. Stacey, N. Dontschuk, K. M. O'Donnell *et al.,* Phys. Rev. X **9**, 031052 (2019).